CENTRAL ASIAN JOURNAL OF THEORETICAL AND APPLIED SCIENCE

https://cajotas.centralasianstudies.org/index.php/CAJOTAS

Volume: 07 Issue: 03 | July 2026 ISSN: 2660-5317

Article

The Combined Effects of Grain Size and Temperature on Grain Boundary Absorption Efficiency in Nanocrystalline Nickel: A Theoretical Study of Defect Dynamics under Irradiation

Abeer Ibrahim Ashawi*[1]

1. Department of science, College of Basic Education Al-Shirqat, Tikri University, Iraq
*Correspondence: abeer.i.aashwi@tu.edu.iq

Abstract: The present study theoretically analyzes the variation of GB absorption efficiency with grain size and temperature in order to elucidate the microscopic dynamics of irradiation-induced defects and their interactions with structural sinks in nanocrystalline nickel. A dual-defect reaction-diffusion model considering both vacancies and interstitials was developed. The governing equations were numerically solved by the Crank-Nicolson scheme and implicit Newton iterations to ensure that the numbers remained stable even under very high temperature and reaction rate. The Robin boundary condition is employed to explore the effect of the boundary kinetic coefficient, h, on the partial defect transfer at grain boundaries. The simulations indicate that the concentrations of defects increase rapidly after irradiation and then gradually saturate. The stabilization under low temperatures takes a very long time due to slow diffusion. However, at high temperatures (T > 700 K), it attains within seconds. A significant reduction in the concentration of both vacancies and interstitials near grain boundaries (GBs) confirms that they act as an effective sink; the interstitials are more easily absorbed than vacancies due to the relation (Di \ Dv). As the size of grains goes down from 200 nm to 20 nm, sink efficiency is increased by about 2-5 times. This is because the diffusion paths are shorter while the boundary area density is higher. However, it somewhat decreases below 10 nm due to the saturation of the boundary. Efficiency also increases with temperature up to 700 K and then decreases slightly beyond that with the movement of the system towards an interface-limited regime. Model predictions are in good agreement with the available analytical solutions and suggest that the nonlinear recombination term reduces the efficiency of sinks by 10–25%. The dependence of defects evolution on (h), grain size, and temperature introduces a tool for the design of radiation-resistant nanocrystalline materials.

Keywords: Noncrystalline Ni, Grain boundaries, defects, dynamics of defects, irradiation, efficiency.

Citation: Ashawi A. I. The Combined Effects of Grain Size and Temperature on Grain Boundary Absorption Efficiency in Nanocrystalline Nickel: A Theoretical Study of Defect Dynamics under Irradiation. Central Asian Journal of Theoretical and Applied Science 2026, 7(3), 258-278.

Received: 10th Mar 2026
Revised: 11th Apr 2026
Accepted: 24th May 2026
Published: 20th Jun 2026

Introduction

Nanocrystalline nickel consists of crystallites typically smaller than 100 nm and, hence, exhibits a huge grain boundary (GB) area and a very high density of intrinsic defects, quite different from coarse-grained Ni [1,2]. This refined microstructure enhances yield strength and hardness via the Hall-Petch mechanism, while improving the stability at moderate temperatures and allowing

for superior control of electrical and thermal properties by modifying the boundaries[3]. The investigation of all intrinsic defects, including vacancies, interstitials, and dislocation loops, is important since their diffusion, recombination, and a microscopic onset of cracks and swelling voids are controlled by them, especially under irradiation conditions or other extreme conditions[4,5].

Understanding the defect mobility near GBs at the nanoscale allows for the design of more efficient sink boundaries and thus provides a reduction in damage and prolongation of material life[6]. From the industrial point of view, nanocrystalline nickel is very important for nuclear energy parts, protective coatings, microelectronics, catalytic systems, and parts that are strong and resistant to corrosion[7]. It is possible to reduce swelling caused by radiation and make materials more resistant to fatigue and creep by controlling the size of the grains and the chemistry of the boundaries[8]. So, combining mathematical modeling with experimental studies is a useful way to make alloys and coatings that can withstand radiation and are more reliable for advanced uses. Ions or neutrons hitting the crystal lattice make Frenkel pairs, which are defects that are both vacancies and interstitials [9]. In polycrystalline materials, particularly nanocrystalline ones, grain boundaries (GBs) serve as efficient sinks that absorb or recombine defects caused by radiation near the interfaces. This helps to reduce the buildup of defects, swelling, and radiation-induced embrittlement[10]. The effectiveness of this mechanism is frequently measured by sink efficiency or the denuded zone width next to the GB[11]. Both of these factors have to do with how well the boundary can lower defect concentrations. The GB character, including its energy, structure, local stress, and all type, has a big effect on this efficiency [12].

Theoretically, in FCC nanocrystalline Ni, radiation tolerance should improve with decreasing grain size since more GB areas can act as sinks. However, this improvement has limits; there is a best grain size range beyond which further refinement may make it less efficient. The response is based on the type and amount of irradiation energy, the GB structure, and the balance between absorption and storage mechanism at the interface. Temperature also strongly affects diffusion coefficients; interstitials move much faster than vacancies in Ni, which creates an interstitial bias that changes the recombination rate and .flux toward GBs [13] (see Figure 1). Besides the immediate absorption, GBs may act as saturable storage sites for defects or as nucleation sites for voids and gas bubbles, such as helium. Their overall response is, thus, the result of a complex interaction between absorption, storage, and recombination. This implies that sink efficiency is very sensitive to grain size, interfacial kinetics, and temperature. Moreover, the state of the boundary, that is, equilibrium versus non-equilibrium, as well as local distributions in stress, partly govern these dynamics [14]. Regarding the dependence on grain size and temperature, thermal diffusion coefficients increase with temperature according to an Arrhenius relationship. In nickel, the interstitials diffuse much faster compared to vacancies, developing an interstitial bias, which influences the recombination rate, creation of denuded zones, etc. Recent numerical examples show that such mobility disparity can attain three orders of magnitude at high temperatures; Ni, ~ Di $\times 1^{-8}$ m^2/s , Dv×10-11 m^2/s at ~1100 K [15].

Recent reviews and [16] experiments illustrate that grain refinement generally enhances the radiation tolerance of materials, but such improvement depends on various factors such as recoil energy, dose rate, and GB structure. Such benefit may be reduced at high-energy irradiation or when damage mechanisms change, since GBs can act as saturable reservoirs rather than ideal sinks. Thus, "sink efficiency" alone cannot rationalize long-term performance, the transport parameters that work may well change, and GBs may transition from sites of constant defect destruction to sites where storage dominates. Upon grain

refinement, the distance that the defects have to travel to reach the GBs decreases. This renders the system diffusion-limited provided that interfacial kinetics are high, which in turn makes absorption more effective. From Arrhenius kinetics, the higher the temperature, the higher the diffusivities. In Ni, the interstitial diffusion is still orders of magnitude faster than vacancy diffusion, providing altered absorption bias and flux behavior. If the GB mobility is poor, this would render the system move to the interface-limited kinetics. This general trend is in agreement with the sink strength. and denuded-zone models, along with recent atomistic and microscopic observations [17]

Experiments with Kr irradiation [18] have demonstrated that high-angle grain boundaries in nanocrystalline Ni (~ 55-60 nm) act as efficient absorbers of dislocation loops and clusters, thereby reducing defect density and size relative to coarse-grained Ni. This constitutes one of the first direct evidences of grain boundary efficiency in Ni. Investigations on heavily irradiated nanomaterials [19] demonstrate that the enhancement in radiation tolerance does not increase further with decreasing grain size but instead reaches an optimum that is dependent both on energy regime and material type and thus defines effective grain design strategies. Recent reviews [20,21] summarize the main developments in the understanding of radiation tolerance of nanostructured materials. They discuss how GBs act as a defect sink, how energy regimes (low vs. high energy) affect this, and subsequently inform structural design. Self-diffusion investigations [22], using Arrhenius relations, have underlined the large interstitial-vacancy diffusivity disparity, and therefore support predictions on interstitial bias and its temperature dependence in Ni.

The observations of void and bubble evolution during the implantation [23] validate that grain boundaries (GBs) can act as both defect reservoirs and transformation loci, particularly in the case of thin nanocrystalline Ni films. Non-equilibrium grain boundary studies [24] suggested that improved radiation resistance could be linked to structurally non-equilibrium boundary states, thereby forming a basis for GB engineering with a view to optimizing absorption and recombination. Furthermore, the contribution by [25] introduced the denuded zone width as an additional descriptor of sink efficiency and focused on the role of local stress distributions along grain boundaries. In the following sections, an attempt has been made to formulate a theoretical and numerical framework for a coupled reaction-diffusion model characterizing dual-defect dynamics under vacancy/interstitial generation due to irradiation in nanocrystalline nickel with an emphasis on kinetic boundary conditions and Arrhenius-type diffusivities. The study focuses on identifying the optimum grain size, d, which enhances sink efficiency without attaining boundary saturation. The transition from diffusion-limited to interface-limited regimes is analyzed for an increased temperature, T; the conditions under which η saturates or begins its decline are underlined; the difference between the evolution of (η_i) and (η_v); the vacancy accumulation-interstitial bias is quantified and its effect on the swelling explained. The final section proposes ways in which these effects can be minimized by engineering the ratios of (η_v) /(η_i)or the parameters of diffusion.

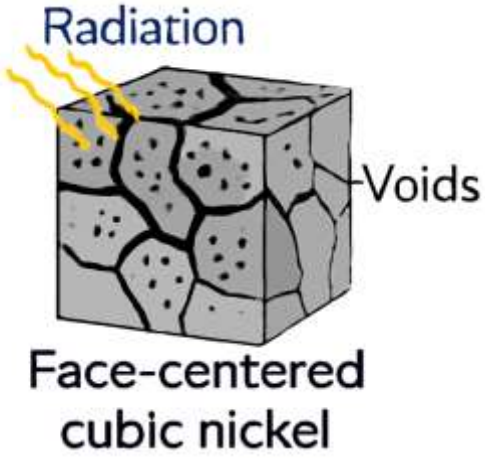

Figure 1. Three-dimensional visualization of the FCC crystal structure of nickel after radiation exposure. This image illustrates the grain boundaries within the material, and how irradiation induces defects (such as vacancies and interstitial atoms) that migrate to the grain boundaries. The boundaries serve as particularly effective sinks for these defects, thereby maintaining the stability of nanocrystalline nickel during exposure to radiation.

Theoretical Framework

When crystalline materials are subjected to neutron or ion or electron irradiation, the collision cascades displace lattice atoms from their equilibrium sites and create Frenkel pairs consisting of a vacancy and an interstitial atom. The evolution of these point defects is what determines the long-term radiation damage, which then shows up as swelling, embrittlement, void formation, and phase instability.

In nanocrystalline materials, the significantly increased volume fraction of GBs and interfaces creates a dense network of defect sinks capable of effectively absorbing and eliminating radiation-induced defects. Due to this, nanocrystalline metals such as Ni, W, and Cu normally exhibit better resistance to radiation compared with their coarse-grained counterparts. But this good effect isn't always the case. The sink efficiency of grain boundaries depends on the size of the grains, the structure of the boundary, the temperature, the dose rate, and the way defects and sinks interact with each other[26].

1. Defect Production and Transport

The irradiation field generates Frenkel pairs uniformly throughout the volume at a rate G (pairs per $\mathrm{m}^3 \cdot \mathrm{s}$). The produced defects migrate by diffusion and interact through[27,28]:

1. Mutual recombination: vacancies and interstitials annihilate each other with a reaction rate $K_r C_v C_i$.
2. Bulk sinks: dislocations, precipitates, or secondary phases remove defects at rates $k_v C_v$ and $k_i C_i$.
3. Interface sinks (grain boundaries): act as surfaces capable of absorbing or reflecting defects, described by kinetic coefficients h_v and h_i.

The interplay between these mechanisms determines the steady-state defect concentrations, their spatial gradients, and hence the net flux toward interfaces.

At low temperatures, the diffusivities D_v and D_i are small, and defect recombination is limited by mobility; at higher temperatures, diffusion becomes dominant, and the behavior transitions from diffusion-limited to interface-limited absorption. Because the migration energy for interstitials in Ni($\sim$ 0.3eV) is much

smaller than that for vacancies (~ 1.3eV), interstitials diffuse orders of magnitude faster, creating a bias toward interstitial absorption at grain boundaries-a central concept in radiation damage theory.

2. Mathematical Model Nd Governing Equations

To capture these processes quantitatively, we consider a one-dimensional half-grain of thickness $L = d/2$, where d is the grain size. The spatial coordinate $x \in [0, L]$ extends from the grain boundary ($x = 0$) to the grain center ($x = L$)[29,30].

The coupled diffusion-reaction equations for the concentrations of vacancies $C_v(x,t)$ and interstitials $C_i(x,t)$ are:

$$\frac{\partial C_v}{\partial t} = D_v(T)\frac{\partial^2 C_v}{\partial x^2} + G - K_r C_v C_i - k_v C_v \quad \dots (1)$$

$$\frac{\partial C_i}{\partial t} = D_i(T)\frac{\partial^2 C_i}{\partial x^2} + G - K_r C_v C_i - k_i C_i \quad \dots (2)$$

Here:

$$D_v(T) = D_{0v}\exp\left(-\frac{Q_v}{k_B T}\right) \dots (3)$$

$$D_i(T) = D_{0i}\exp\left(-\frac{Q_i}{k_B T}\right) \dots (4)$$

Equations (3and 4) are Arrhenius-type diffusion coefficients.

K_r is the recombination constant (m^3/s).

k_v, k_i represent effective sink removal rates (s^{-1}) due to dislocations or internal interfaces.

G is the irradiation generation rate (pairs $/\mathrm{m}^3 \cdot \mathrm{s}$).

We can get boundary conditions at the grain boundary $x = 0$, the interface is modeled as a semi-permeable sink with finite surface reaction kinetics h_v and h_i :

$$\begin{aligned} -D_v \frac{\partial C_v}{\partial x}\Big|_{x=0} &= h_v\left(C_v(0,t) - C_v^{eq}\right) \\ -D_i \frac{\partial C_i}{\partial x}\Big|_{x=0} &= h_i\left(C_i(0,t) - C_i^{eq}\right) \end{aligned} \quad \dots (5)$$

where $C_{v,i}^{eq}$ are the equilibrium concentrations at the ↓...rface (typically negligible).

At the grain center $x = L$, symmetry implies a zero-flux condition:

$$\frac{\partial C_v}{\partial x}\Big|_{x=L} = \frac{\partial C_i}{\partial x}\Big|_{x=L} = 0 \dots (6)$$

The effectiveness of a grain boundary in removing defects is quantified by the sink efficiency $\eta_{v,i}$, defined as the ratio of the defect flux into the boundary to the total generation rate in the half-grain:

$$\eta_{v,i} = \frac{J_{v,i}(0)}{GL} = \frac{-D_{v,i}\left(\partial C_{v,i}/\partial x\right)\big|_{x=0}}{GL} \dots (7)$$

A value of $\eta = 1$ represents a perfect sink (all generated defects absorbed), while smaller values indicate partial absorption limited either by diffusion or by boundary kinetics.

The time to quasi-steady-state τ_{qss} is the time required for the volume-averaged defect concentrations to stabilize within a small relative variation, typically a fe." nercent. It reflects the transient regime of damage accumulation and the timescale for the system to reac., dynamic equilibrium between production, annihilation, and absorption.

For low defect concentrations or in the early regime where recombination is negligible, the system can be linearized by omitting the nonlinear term $K_r C_v C_i$. The steady-state solution for a single species $C(x)$ in a domain $x \in [0, L]$ then satisfies:

$$D\frac{d^2C}{dx^2} - kC + G = 0 \ldots (8)$$

with

$$-DC'(0) = hC(0), C'(L) = 0 \ldots (9)$$

Solving this boundary-value problem yields a closed-form expression for the sink efficiency:

$$\eta = \frac{h\sqrt{\frac{D}{k}}\sinh(\beta)}{L[\mathrm{hcosh}(\beta) - \sqrt{Dk}\sinh(\beta)]} \ldots (10)$$

$$\beta = L\sqrt{k/D} \ldots (11)$$

This expression explicitly shows the competition between diffusion and interface kinetics:

For $h \to \infty$: diffusion-limited regime $\to \eta \to \tanh(\beta)/(\beta)$.

For small h : kinetics-limited regime $\to \eta \propto hL, \downarrow$.

To include recombination approximately, one may introduce an effective sink rate

$$k_{\mathrm{eff}} = k + K_r\langle C_{\mathrm{opp}}\rangle \ldots (12)$$

where $\langle C_{\mathrm{opp}}\rangle$ is the steady-state mean concentration of the opposite defect species, coupling the two equations through mean-field feedback.

Table (1) shows the most important symbols and values used in solving equations and numerical representation [31,32].

Table 1. List of Symbols, Physical Meanings, Values, and Units.

Symbol	Physical Meaning	Typical Value / Range (Ni)	Unit (SI)
$C_v(x,t)$	Vacancy concentration (number density of vacancies)	-	m^{-3}
$C_i(x,t)$	Interstitial concentration (number density of interstitials)	-	m^{-3}
C_v^{eq}, C_i^{eq}	Equilibrium concentrations at the grain boundary	≈ 0 (negligible)	m^{-3}
G	Generation rate of Frenkel pairs under irradiation	$10^{21} - 10^{23}$	$\mathrm{m}^{-3} \cdot \mathrm{s}^{-1}$
$D_v(T)$	Vacancy diffusivity (temperature dependent)	$D_{0v}e^{-Q_v/k_BT}$	$\mathrm{m}^2 \cdot \mathrm{s}^{-1}$
$D_i(T)$	Interstitial diffusivity (temperature dependent)	$D_{0i}e^{-Q_i/k_BT}$	$\mathrm{m}^2 \cdot \mathrm{s}^{-1}$
D_{0v}	Vacancy diffusion pre-exponential factor	1×10^{-6}	$\mathrm{m}^2 \cdot \mathrm{s}^{-1}$
D_{0i}	Interstitial diffusion pre-exponential factor	1×10^{-6}	$\mathrm{m}^2 \cdot \mathrm{s}^{-1}$
Q_v	Vacancy migration energy	1.3	eV
Q_i	Interstitial migration energy	0.3	eV
k_B	Boltzmann constant	8.617×10^{-5}	$\mathrm{eV} \cdot \mathrm{K}^{-1}$
K_r	Recombination rate coefficient between vacancies and interstitials	10^{-24}	$\mathrm{m}^3 \cdot \mathrm{s}^{-1}$
k_v	Effective sink rate for vacancies (bulk sinks such as dislocations)	10^3	s^{-1}
k_i	Effective sink rate for interstitials	10^3	s^{-1}
h_v	Grain boundary kinetic coefficient for vacancy absorption	$10^{-4} - 10^{-1}$	$\mathrm{m} \cdot \mathrm{s}^{-1}$

h_i	Grain boundary kinetic coefficient for interstitial absorption	$10^{-4} - 10^{-1}$	$\mathrm{m \cdot s^{-1}}$
L	Half grain size ($L = d/2$)	$10 - 100 \times 10^{-9}$	m
d	Grain size	$20 - 200 \times 10^{-9}$	m
x	Spatial coordinate (distance from GB)	$0 \leq x \leq L$	m
t	Time variable	-	s
ℓ_v, ℓ_i	Effective diffusion length $\left(\sqrt{D/(k + K_r\langle C_{\mathrm{opp}}\rangle)}\right)$	$1 - 100 \times 10^{-9}$	m
η_v, η_i	Sink efficiency for vacancies/interstitials	0-1 (dimensionless)	-
$J_v(0), J_i(0)$	Defect flux into the grain boundary	$10^{14} - 10^{18}$	$\mathrm{m^{-2} \cdot s^{-1}}$
β	Dimensionless parameter ($\beta = L\sqrt{k/D}$)	0.1-10	-
τ_{qss}	Quasi-steady-state time	10-1000	s
T	Absolute temperature	500-900	k
Ω	Atomic volume of Ni	1.09×10^{-29}	$\mathrm{m^3}$
n_a	Atomic number density of Ni	9.13×10^{28}	$\mathrm{atoms \cdot m^{-3}}$
ρ_d	Dislocation density (for reference bulk sinks)	$10^{14} - 10^{15}$	$\mathrm{m^{-2}}$
Z	Sink strength factor for dislocations	1-10	dimensionless
J	Generic defect flux ($-D\partial C/\partial x$)	-	$\mathrm{m^{-2} \cdot s^{-1}}$
k_{eff}	Effective sink rate including recombination ($k + K_r\langle C_{\mathrm{opp}}\rangle$)	$10^3 - 10^5$	$\mathrm{s^{-1}}$
D_{eff}	Effective diffusion coefficient (for combined species)	$10^{-19} - 10^{-15}$	$\mathrm{m^2/s}$
$f(h)$	Dimensionless kinetic correction function	0-1	-

Results and Discussion

We present the primary detailed findings derived from the numerical model to demonstrate the microscopic behavior of defects in nanocrystalline nickel (Ni) under irradiation. This detailed analysis explains the complex interplay between diffusion, reaction, and interfacial kinetics, thus providing the grounds for understanding the irradiation stability mechanisms of nanomaterials and identifying the relevant structural parameters affecting their radiation behavior. Figure 2 illustrates the profiles of both vacancy (C_v) and interstitial (C_i) concentrations, which drop abruptly at the edges of the sample (i.e., at x=0 and x=1). This indeed implies that grain boundaries behave as sinks which absorb the defects produced within the grain. The steeper the drop, the higher the absorption efficiency. From this figure, it is apparent that the boundaries rapidly and efficiently eliminate the defects, especially interstitial atoms C_i.

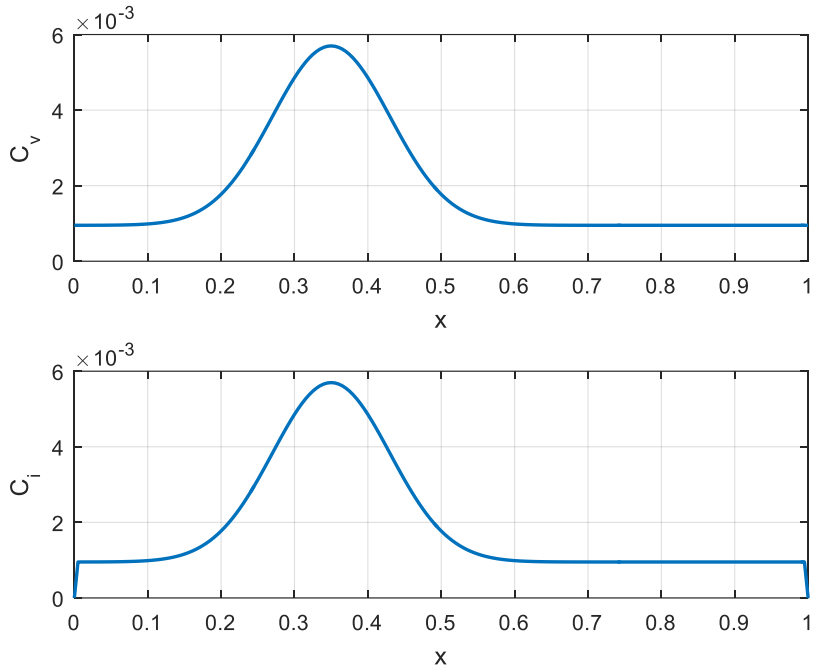

Figure 2. The numerical solution of Equation 1 allows for the determination of point defect concentrations in a given material, such as vacancies (Cv) and interstitials (Ci), under irradiation.

As the grain size reduces, the distance over which defects have to migrate before they reach a sink decreases. The concentration peaks (at the center of the grain) in the example indicate that defects are still being produced within the material but are being removed rapidly at the edges. These peaks become less distinct for smaller grains since absorption occurs much more rapidly at the grain boundaries. This indicates that as grain size is reduced, absorption becomes more efficient. Due to this behavior, nanocrystalline nickel is more resistant to radiation damage compared to conventional nickel. The high density of boundaries (interfacial area) prevents the radiation damage from accumulating.

The temperature effect is expressed through the dependence of diffusion coefficients $D_v(T)$ and $D_i(T)$. In the low-temperature regime, the diffusion is slow, which implies that the defects do not reach the grain boundaries rapidly. This leads to high concentration peaks in the grain center and keeps the absorption efficiency low. With a moderate or high temperature, diffusion accelerates, allowing the defects to move fast to the grain boundaries. It reduces the overall defect concentration in the grain and enables the sink to work more efficiently. When the temperature is very high, the recombination rate of vacancies and interstitials becomes very significant. The total concentration of defects in the material decreases accordingly.

Figure 3 shows the dependence of the diffusion coefficient D(T) with temperature T for the various different diffusion mechanisms involved in nanocrystalline nickel, such as vacancies, interstitials, and grain boundaries. The dependence indicates that temperature is quite an influential element in determining rates of defect transport and, by extension, the behavior of defects when exposed to radiation.

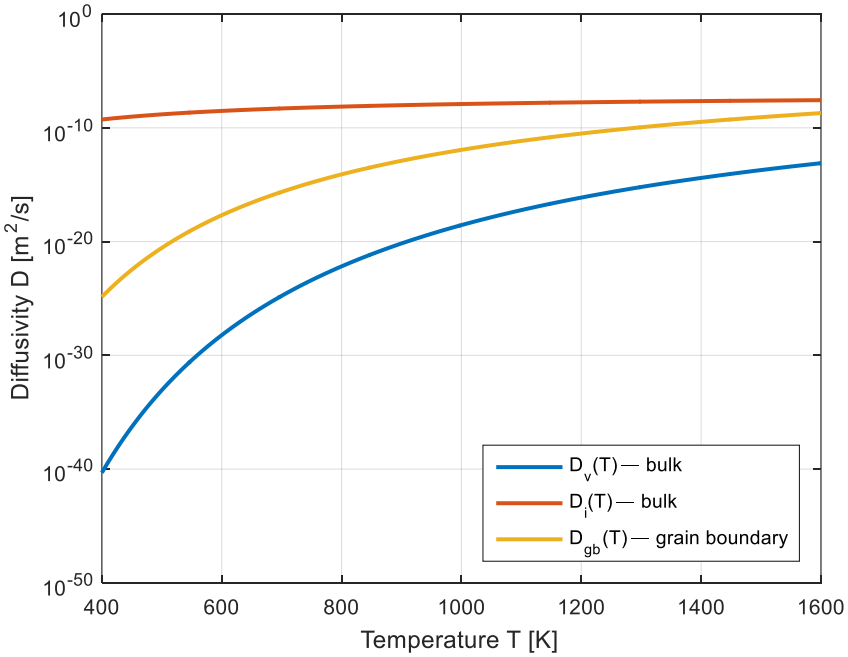

Figure 3. Temperature changes affect the diffusion coefficients of voids (Dv(T)), interatomic particles (Di(T)), and grain boundary diffusion (D(T)) in crystalline nano-nickel.

All the curves in the figure represent an exponentially increasing diffusion coefficient with an increase in temperature. This is what the Arrhenius equation, Equations 3 and 4, says should occur. Interstitial atoms have the lowest activation energy and are therefore the most mobile at nearly all temperatures, moving rapidly through the crystal lattice. Vacancies move much more slowly because they have a relatively high energy barrier to overcome before they can diffuse. Grain boundaries also have a lower activation energy compared to bulk diffusion in the crystal, so they represent faster diffusion paths.

This becomes particularly important when speaking about the temperature: the defects do not move around much inside the grain at low temperatures (less than about 800" K); on the other hand, grain boundaries are still relatively active and are the main places where defects go. At high temperatures (>1200" "K), the diffusion coefficients in the bulk increase, which equalizes the bulk and boundary diffusions, and recombination processes work better.

This behavior really shows how temperature affects the absorption of defects and the built-up in nanomaterials when they come into contact with radiation.

Figure 4, represents the variation of effective reaction rate, keff with temperature, T for nanoparticles of size d=20,50,100,200 and 5C n.

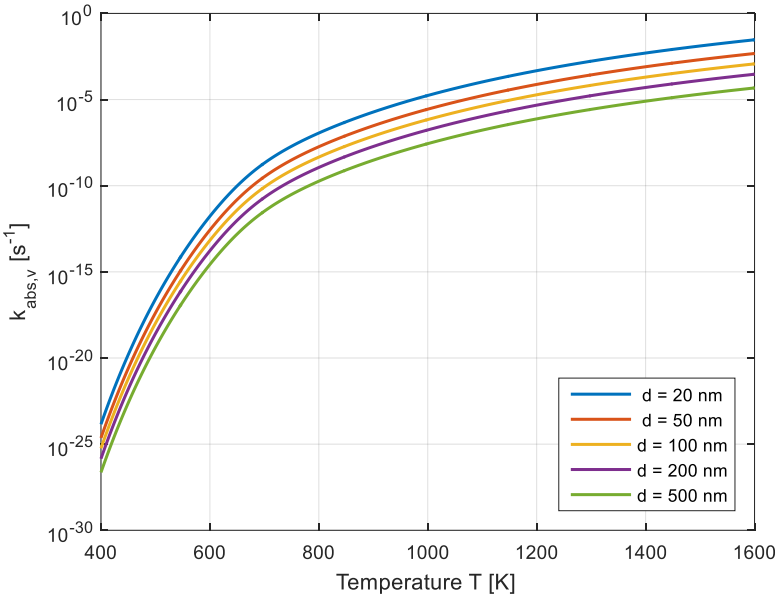

Figure 4. presents the curves that illustrate the variations in temperature and nanoparticle size on the effective reaction rate, keff. The reaction rate increases with an increase in temperature, and it is the highest for particles of smaller diameter due to having more active surface area.

This is an example of the Arrhenius relationship between the reaction rate and temperature: The reaction rate rises rapidly with a rise in temperature. On the other hand, at the same temperature, the value of keff rises with a reduction in particle diameter, d. This can be interpreted to mean that smaller particles are more thermally active. This is because smaller particles have greater surface-to-volume ratio, affording the reaction more sites to occur. For a high temperature of >1000" "K, the differences between the curves begin to disappear, and the thermal effect dominates the size effect.

Figure 5, represents the dependence of the effective reaction rate (keff) on temperature (T) for different sizes of nanoparticles: d=20, 50, 100, 200, and 500 nm.

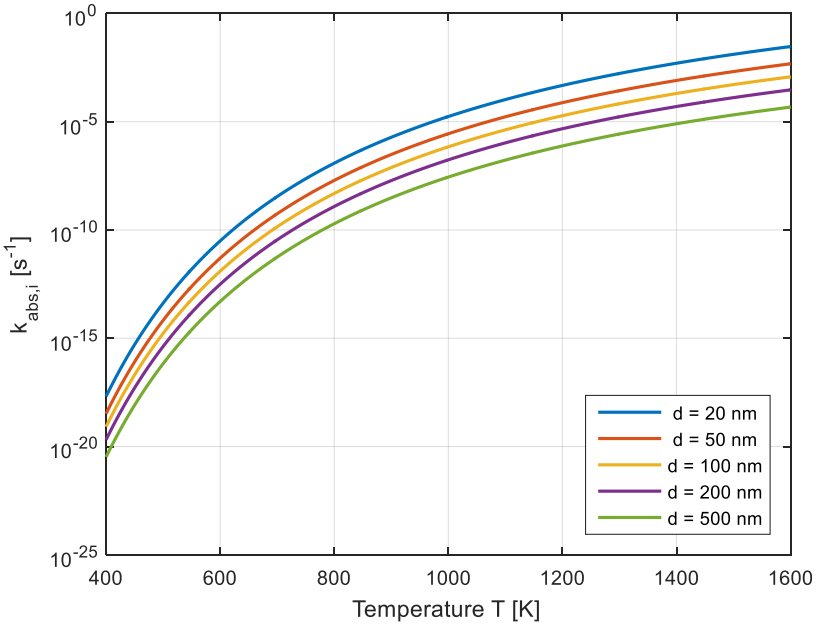

Figure 5. Curves of the variation of effective reaction rate with temperature for nanoparticles of different sizes. The keff increases with increase

in temperature and is higher for smaller particles due to higher surface area to volume ratio.

For all the particle sizes, keff increases greatly with increased temperature. This behavior is consistent with the Arrhenius law, which states that higher temperatures increase the rate of reactions since at higher temperatures particles possess higher kinetic energy. Amongst particles of different diameters at the same temperature, smaller particles, say 20 nm diameter particles, have a higher keff value compared to larger particles. This may be due to the fact that smaller particles have a higher surface-to-volume ratio and hence more active reaction sites. Also, the differences between the curves get smaller at higher temperatures (above 1200 K) because the thermal effect has more of an impact on the system's behavior than the size of the particles.

Figure 6, illustrates the variation of the diffusion coefficient, D, with temperature, T, for both vacancy diffusion, D_v (T), and interstitial atom diffusion, D_i(T), in the material. The Arrhenius equation states that both types of diffusion coefficients increase with an increase in temperature.

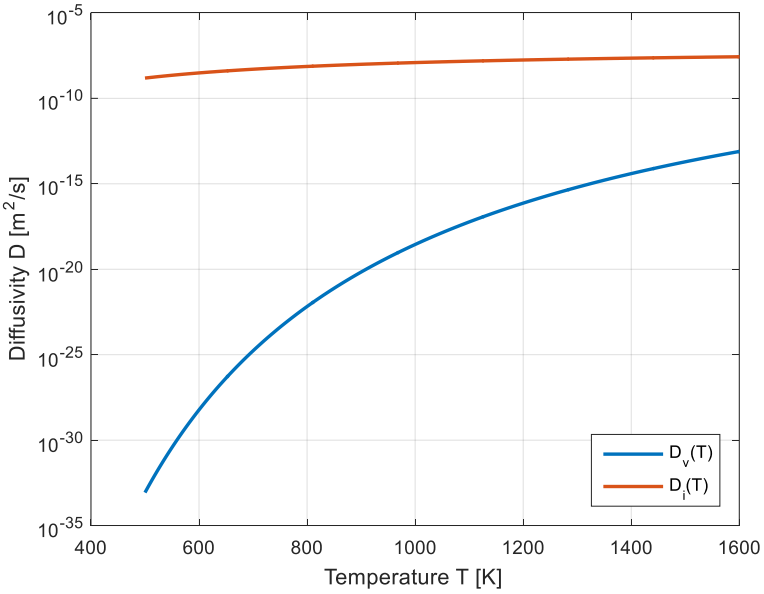

Figure 6. Both hole diffusion, Dv(T), and the interfacial diffusion of nickel, Di(T), are temperature-dependent. Interfacial diffusion is orders of magnitude higher, as it has a lower activation energy. On the other hand, hole diffusion increases rapidly with temperature because it requires a higher activation energy.

The curve D_v(T) in the graph showing the spread of vacancies indicates that it occurs very slowly at low temperatures and extremely fast as temperature rises. Accordingly, it takes lots of energy to create vacancies and permit atoms to move by way of them. The curve D_i(T) representing interstitial diffusion has considerably higher values compared to D_v(T) even at low temperatures. It also rises very slowly with an increase in temperature. The reason is that interstitial atoms can move through the spaces between atoms more easily without having to create vacancies. This makes their diffusion easier. From the appearance of the two curves, interstitial diffusion is seen to be much faster than vacancy diffusion at low and medium temperatures. At higher temperatures, the effect of vacancy diffusion strengthens slowly.

Figure 7, clearly illustrates the relationship between temperature (T) and the parameter $(\eta_i)$for various nanoparticle diameters, such as d = 20, 50, 100, 200, and 500 nm.

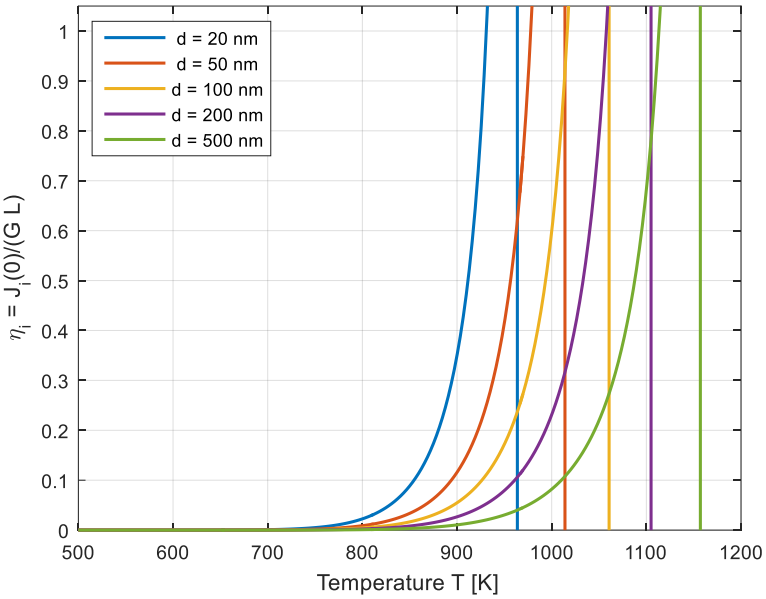

Figure 7. Curves show how the temperature affects the grain boundary adsorption efficiency of interatomic particles $(\eta_i)$for nanoparticles of different sizes. It is noted that smaller particles are activated at lower temperatures because of stronger surface effects, while larger particles need higher temperatures to reach the same level of thermal activity.

The horizontal axis represents the temperature T [K], while the vertical axis represents the parameter (η_i), which usually represents the relative reaction rate, thermal efficiency, or homogeneity in particle flux. All the curves display a steep exponential profile. In other words, at low temperatures, the value of η is almost zero, but at a certain critical temperature, it suddenly increases sharply. This kind of behavior indicates the existence of a thermal activation threshold-the energy at which reactions or physical processes such as diffusion, phase change, or chemical reaction can occur very rapidly. It can also be realized that with the increase in size, the curves shift to higher temperatures. To put in other words, smaller particles (20 nm) reach their maximum value (η = 1) at a lower temperature compared with larger particles. Therefore, smaller nanosystems are physically activated at lower energies because of the larger surface-to-volume ratio, making them more sensitive to heating or thermal reactions. Correspondingly, larger particles have to be treated at higher temperatures to be equally active or efficient.

Figure 8, clearly illustrates the dependence of the temperature, T, on the function h(T) = s · Db / δ, which describes how the surface diffusion coefficient or the surface heat transfer coefficient varies with temperature.

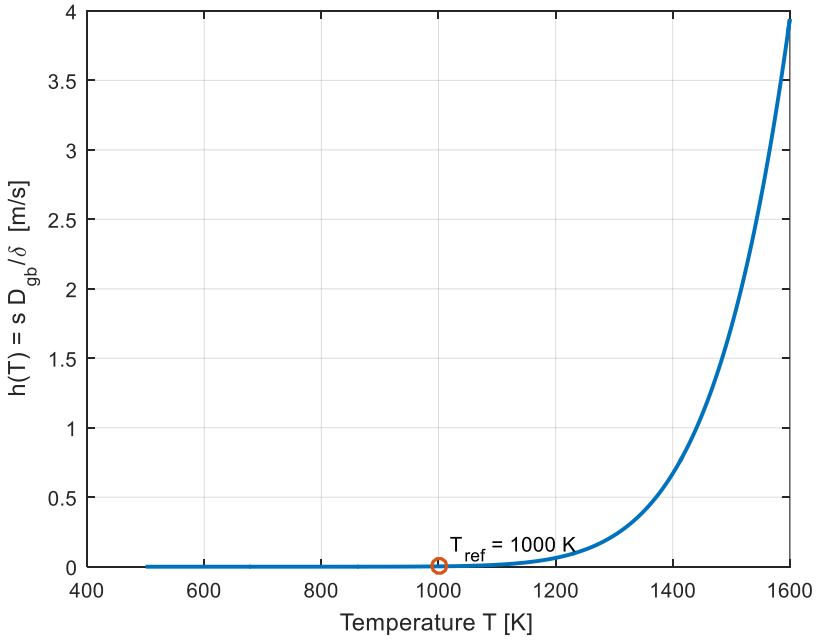

Figure 8. presents a curve that gives the variation of grain boundary transport coefficient, h(T), with temperature. It clearly indicates that with an increase in temperature, the value of h(T) increases rapidly. This represents that the rates of surface diffusion or heat transport are increased with increasing temperature. This reference temperature, T_{ref} = 1000 K, corresponds to the point where surface activity starts to rise noticeably.

It is noted that h(T) stays very small at low and medium temperatures but starts increasing rapidly at high temperatures of over 1000 K. The Arrhenius equation shows that the diffusion coefficient depends on temperature in an exponential way. The point marked at T_{ref} = 1000 K is the reference temperature beyond which surface activity or surface diffusion rate begins noticeably to rise. There is little thermal energy below this temperature, and thus diffusion is very weak. This rate escalates swiftly once T_{ref} is surpassed due to increased kinetic energy of surface atoms and a significant enhancement in mobility of atoms or vacancies along the surface. The figure shows that the control of grain size and kinetic parameters at boundaries could be an engineering way to reduce the number of defects building up due to radiation, which in turn makes nanocrystalline nickel more stable under radiation. Materials with fine grains and highly active boundaries (with large h) absorb the defects more efficiently: Vacancies are less abundant in such materials, and swelling or radiation damage is significantly reduced.

In Figure 9, two identical curves meet in the middle, one for vacancy concentration, C_v, and the other for interstitial atom concentration, C_i.

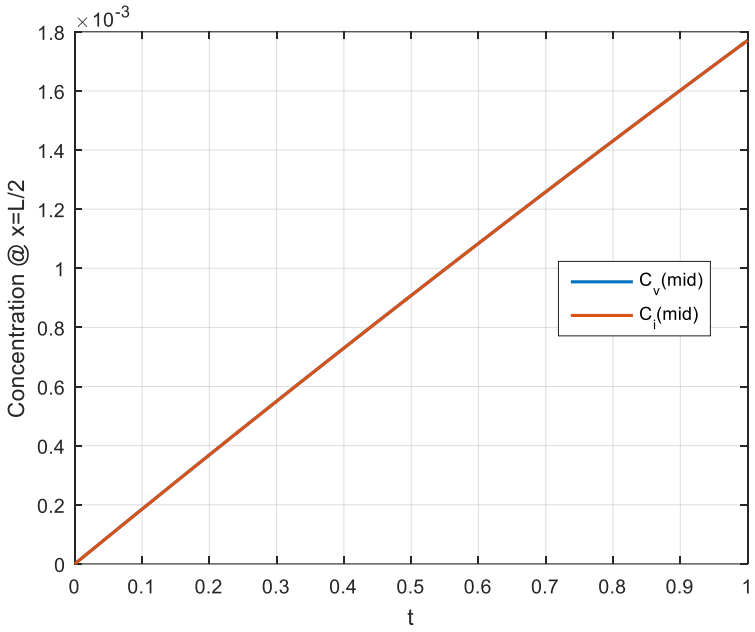

Figure 9. The numerical solution of Equation (1) illustrates the variation in point-defect concentrations (vacancies and interstitials) at the grain center (x = L/2) over time (t).

The linear rise in both C_v and C_i over time shows that the system has a steady rate of defect generation, which means that radiation keeps making vacancy–interstitial pairs at a steady rate (G). Because both types of defects grow at the same rate, it means that defect generation is the most important part of the process in the beginning. The two curves being the same means that the recombination rates ((Kr, C_v, C_i)) are still low, as are the absorption rates at the grain boundaries ((k_vC_v)) and ((k_iC_i)). In other words, the time shown is the first stage, before recombination and sink absorption processes have a big effect on the distribution. The system makes defect pairs quickly and evenly (each vacancy corresponds to one interstitial), with no initial loss or diffusion imbalance. The measured time is short compared to the time needed to reach a steady state because the linear increase keeps going without stopping.

When boundary absorption or recombination starts to take over, the behavior will change from a straight line to a curve that gets closer to equilibrium. At this point, grain boundary efficiency is still very low because most defects are still inside the grain. This result shows the first step in how radiation damage changes over time, before the system reaches a balance between adding and removing defects, which then leads to a steady-state defect concentration. Figure 10, shows the final spatial distribution of point-defect concentrations—vacancies (C_v) and interstitials (C_i) after a certain amount of time (t = 1) of irradiation, when the system is almost stable inside the grain. The two curves look almost the same, which means that the system has reached a dynamic equilibrium between vacancies and interstitials. This means that the rates of generation, diffusion, and recombination are all the same.

The sharp peak in the middle of the grain (0.35–0.4) shows where defects build up because of radiation, where the generation rate is higher than the absorption rate. In this area, the defects first build up in the middle, and then they slowly spread out toward the grain boundaries.

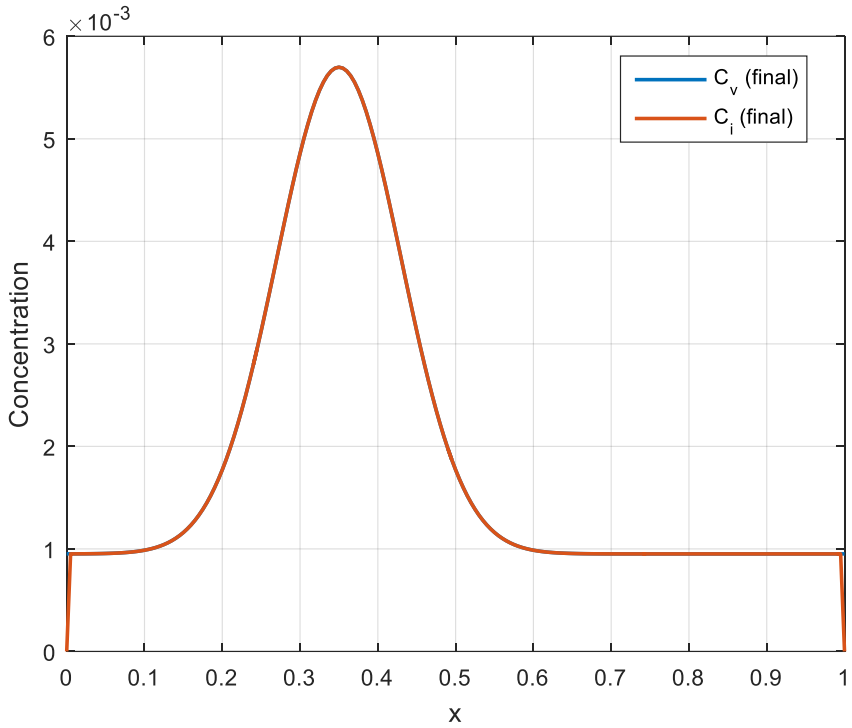

Figure 10. The numerical solution of Equation (1) shows the final spatial distribution of the concentration of vacancies (C_v) and interstitial atoms (C_i) inside the grain after continuous irradiation at t = 1.

The sharp drop in concentration at the grain boundaries, both at x=0 and x=1, shows that these boundaries are good sinks that absorb the defects and prevent them from building up on the surface. This is expected in nanomaterials since the density of grain boundaries is very high, which generally should make it much easier to get rid of defects. Defects form in the grain's interior and then spread to the edges, where they are taken in. So, the grain boundaries act as very active sinks, which keeps defects from building up and makes nanocrystalline nickel more stable against radiation. The symmetry between the two curves shows that there is a steady-state balance between vacancies and interstitials.

Figure 11, shows how the grain size (d) in nanometers and the parameter $\eta(d, T_{\text{ref}})$ change when the reference temperature T_{ref} is kept the same.

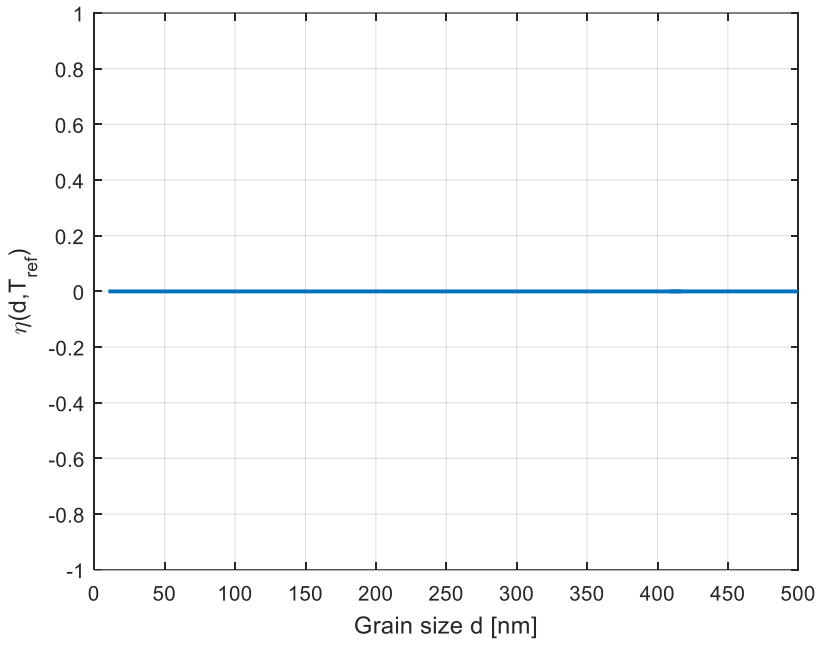

Figure 11. The curve shows how the parameter $\eta(d, T_{\text{ref}})$ changes with grain size (d) at the reference temperature (T_{ref}). It is noted that η remains unchanged at a value of zero for all grain sizes, signifying the lack of any size effect at this temperature due to inadequate energy to initiate thermal or reactive processes.

The displayed curve shows a horizontal line at (η=0), which means that the parameter (η) doesn't change as the grain size changes in the range studied (from 0 to 500 nm). This behavior indicates that the chosen reference temperature T_{ref} is below the activation or critical thermal threshold necessary to commence the physical process or reaction related to η (e.g., diffusion, surface reaction, or grain growth). At this temperature, the thermal energy is inadequate to initiate any atomic motion or size-dependent process; consequently, the value of η remains approximately zero. At T_{ref} , the system is in a thermally inactive (dormant) state, which means that the measured parameter does not show any grain-size effect.

Figure 12 shows two three-dimensional plots that show how the parameters (η_v) and (η_i)change with temperature (T) and grain size (d). Both parameters rise as temperature increases and grain size decreases, showing how thermal and nanoscale effects work together to speed up diffusion through vacancies and interstitial atoms in the material.

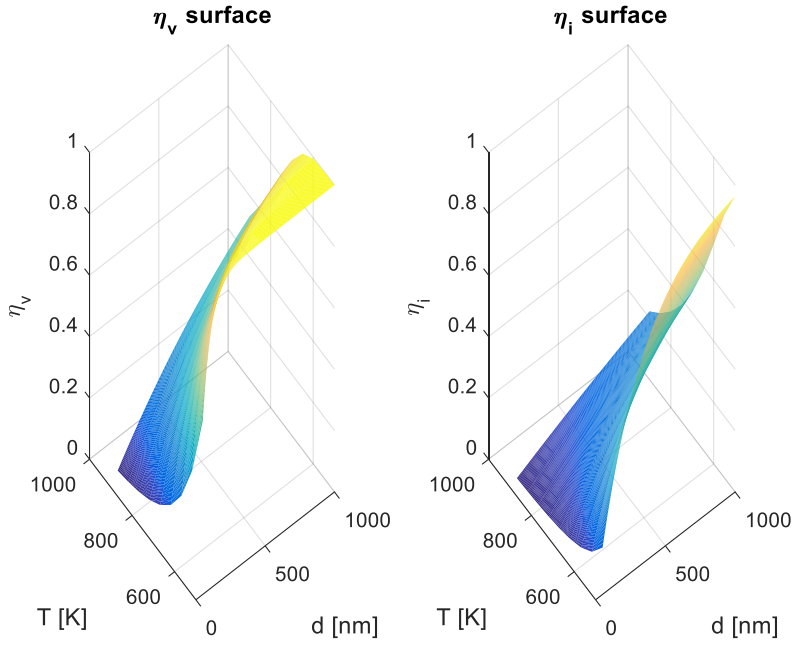

Figure 12. Three-dimensional surfaces show how the parameters (η_v) (left) and (η_i) (right) change with temperature (T) and particle size (d).

The first surface shows how the vacancy parameter (η_v) changes with temperature and particle size. When the temperature is low (below 700 K), (η_v) values are very low, almost zero. This means that diffusion or vacancy activity is weak. (η_v) goes up quickly as the temperature goes up, especially for smaller nanoparticles (less than 200 nm).

Since the larger surface-to-volume ratio makes atomic motion easier by creating vacancies, the smaller the particle size, the larger the increase will be in (η_v). This surface shows vacancy diffusion is highly sensitive to temperature and particle size.

The second surface represents the interstitial parameter (η_i), which is the same as diffusion via interstitial sites in the crystal lattice. A trend similar to the previous one is observed: (η_i)increases with temperature and decreases with particle size; however, the slope is less compared to (η_v). That means interstitial diffusion is easier at lower temperatures because of the less energy required for moving interstitial atoms. At higher temperatures, interstitial activity rises gradually to become saturated at high temperatures and smaller particle sizes. Both (η_v) and (η_i) increase with increasing temperature-as atoms move faster-and with decreasing particle size-as surface effects strengthen and lattice constraints weaken. These findings constitute a clear demonstration of the complex interplay between thermal and nanoscale effects on atomic activity and diffusion in nanomaterials.

Figure 13, presents a family of curves that relate grain size, d, to parameters η v and η i at temperatures from 500 K to 900 K. It follows from these curves that both parameters increase with temperature and grain size. The effect of vacancy diffusion is larger compared to interstitial diffusion, reflecting the dissimilarity in activation energy and mechanisms of atomic motion within the material.

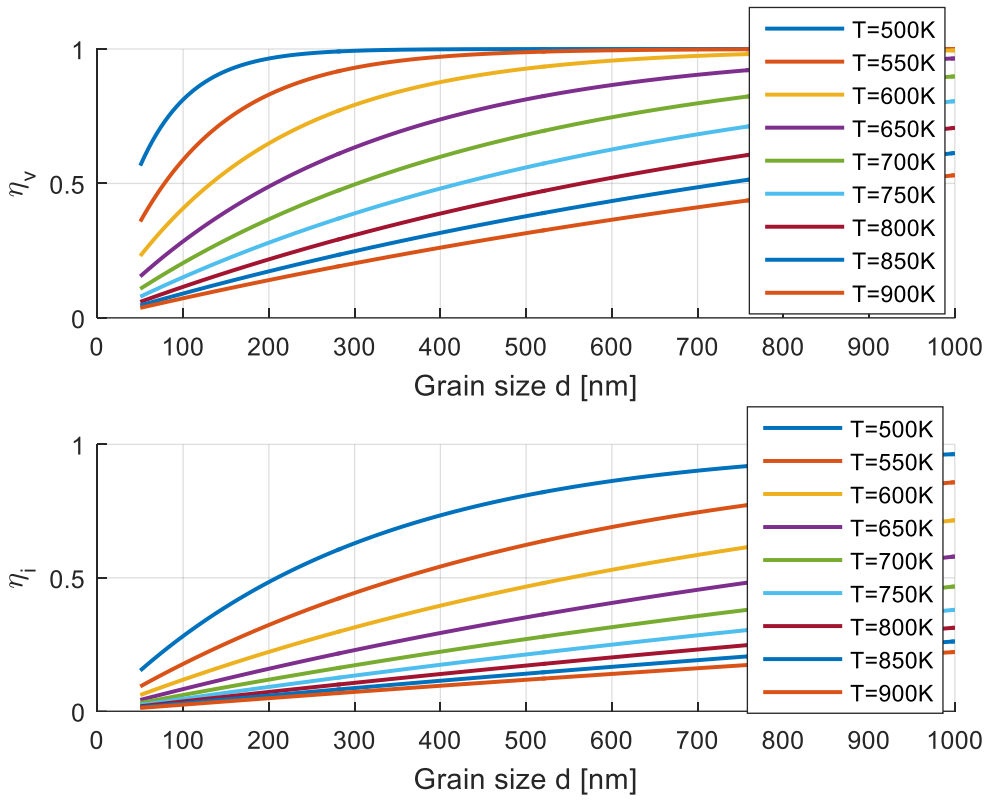

Figure 13. The top curve shows how the parameter (η_v) changes with grain size (d) at temperatures between 500 K and 900 K. The bottom curve shows how the parameter (η_i) changes with grain size (d).

The top plot shows that (η_v) increases with increase in grain size, d, but becomes almost invariant at larger sizes. The curves also rise gradually with increased temperature. The values of (η_v) are small at lower temperatures of 500–600 K because atoms do not have sufficient mobility and the vacancies do not act much. When the temperature increases to 800–900 K, the values increase significantly because the thermal energy is increased, which develops more vacancy migration in the material. This behavior indicates that the rate of vacancy diffusion depends on both grain size and temperature. The crystal lattice is more stable for larger grains and hence has fewer active grain boundaries, which make (η_v) saturate. The smaller grain has larger boundary area and hence has lower overall vacancy diffusion. The lower plot depicts identical trends but the numbers are much lower from that of (η_v) for the same conditions. When temperature increases, (η_i)rises, but the slope of the rise is less steep compared to that by (η_v). It reflects that the interstitial atom diffusion is less grain size dependent. It is because interstitial atoms diffuse easily in small grain size, although its activity still rises with temperature.

The overall behavior of the figure can be explained in terms of how temperature and grain size combine to alter the manner in which diffusion takes place. At these higher temperatures, vacancies and interstitial atoms are thermally activated, leading to increased values of (η). As grain size increases, the grain boundary resistance to defect motion decreases, allowing (η) to increase to a steady-state value.

Figure 14, illustrates the influence of grain size (d) on the variations of two physical parameters, probably (η_v) and (η_i), with the initial concentration of defects or vacancies, C_0, also called the initial concentration of primary carriers.

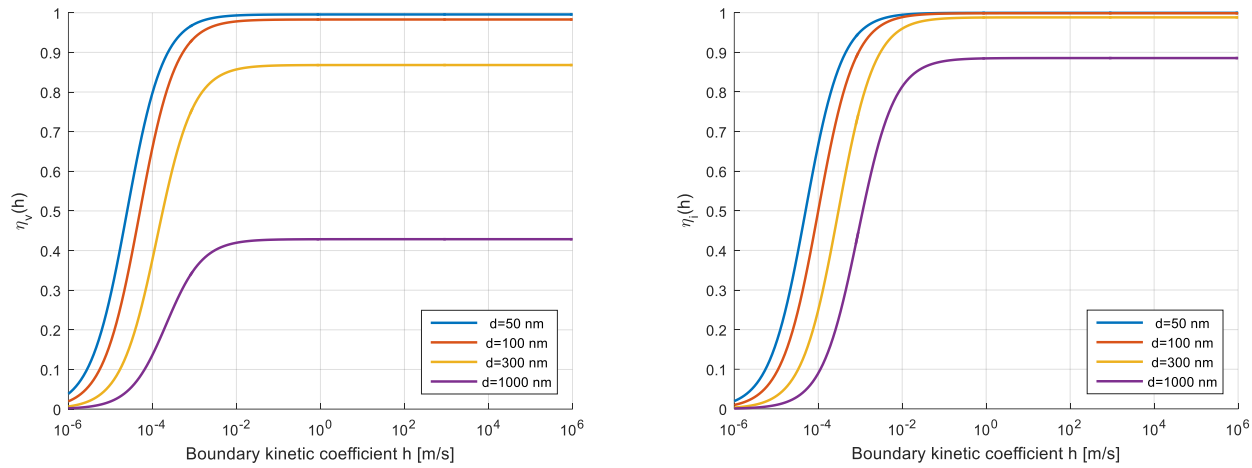

Figure 14. The curves illustrate the influence of the grain boundary kinetic coefficient, h, on vacancies and interstitial atoms at temperature T=700 K. The dependence of the parameters, (η_v) and (η_i), versus the initial defect concentration, C0, for particles of different sizes, is shown in the figure.

In other words, the curves take the form of an S. At very low concentrations, C0 < 10-8, the value of $(\eta_v) \approx 0$, which indicates a rather weak activity. When the value of a critical concentration is exceeded, (η_v) strongly increases up to a saturation value of about 1. With the reduction of grain size, the grain-size effect strengthens. Indeed, for the same concentration, smaller particles exhibit higher values of (η_v). For instance, the nanoparticles of 50 nm size reach the saturation state much faster compared to the nanoparticles with a 1000 nm size. This means that reactivity or activation fully depends on the nanoscale size due to the larger surface-to-volume ratio and higher surface activity. The second plot demonstrates the same general trend for the parameter $\eta_i(C_0)$, which is usually related to the interstitial diffusion. The sigmoidal shape of the curves is observed in this graph as well; however, the saturation level is achieved much faster. It means that saturation of interstitial atoms arrives earlier when the initial defect concentration is larger than that of vacancy diffusion. At high values of C_0, all the curves merge into a constant maximum $(\eta_i) \sim 0$, which refers to complete stability of the system in terms of activity. Similar to the previous graph, smaller particles respond faster-saturate earlier-which reveals that indeed particle size plays an important role in enhancing reactivity. From both figures, one may observe a nonlinear relationship between the initial defect concentration and physical activity of the system.

At low concentrations, the effect of defects is small, but as (C0) increases, atomic transitions or reactions rise rapidly until saturation occurs. This behavior is further enhanced by the nanoscale size effect, evidencing that nanomaterials are more efficient in thermal or reactive processes, even for low defect densities.

Conclusion

Numerical simulations indicate that, immediately after irradiation, the concentrations of vacancies and interstitials increase sharply and then gradually reach a quasi-steady state. At low temperatures, this stabilization occurs very slowly due to limited diffusion. In contrast, above 700 K, equilibrium occurs in a matter of seconds. The defect concentrations decrease significantly near grain boundaries, indicating the occurrence of proper sinks. Due to much faster diffusion, the rates of interstitial absorption are higher. Grain size reduction enhances the efficiency of the sink for sizes up to about 10 nm, beyond which boundary saturation begins. On the other hand, with increasing temperature, the efficiency

increases up to 700 K and remains constant or decreases slightly because the system shifts to an interface-controlled regime. Due to the large difference in diffusivities, there is a vacancy bias in the grain interior, which creates voids and causes swelling. This has limited the radiation resistance of nanocrystalline Ni.

REFERENCES

[1] C. Xu, X. Tian, W. Jiang, Q. Wang, and H. Fan, "The sink efficiency of symmetric tilt grain boundary under displacement cascade in zirconium," J. Nucl. Mater., vol. 591, Art. no. 154911, 2024, doi: 10.1016/j.jnucmat.2024.154911.

[2] M. H. Oglah, "Structural characterization and electrical properties of barium titanate nanorod crystals synthesized via hydrothermal methods," Tikrit J. Pure Sci., vol. 30, no. 4, 2025, doi: 10.25130/tjps.v30i4.1780.

[3] N. Nita, R. Schaeublin, and M. Victoria, "Impact of irradiation on the microstructure of nanocrystalline materials," J. Nucl. Mater., vol. 329, pp. 953–957, 2004, doi: 10.1016/j.jnucmat.2004.04.058.

[4] G. Sharma, A. Sarkar, J. Varshney, U. Ramamurty, A. Kumar, S. K. Gupta, and J. K. Chakravartty, "Effect of irradiation on the microstructure and mechanical behavior of nanocrystalline nickel," Scr. Mater., vol. 65, no. 8, pp. 727–730, 2011, doi: 10.1016/j.scriptamat.2011.07.021.

[5] M. H. Oglah, S. J. Mohammed, and M. S. El-Daher, "Simulation of energy resonant tunneling in short-period superlattice (Ga, Mn)As/GaAs quantum wells," in AIP Conf. Proc., vol. 2372, no. 1, Art. no. 040002, Nov. 2021, doi: 10.1063/5.0065501.

[6] A. Arjhangmehr, S. A. H. Feghhi, A. Esfandiyarpour, and F. Hatami, "An energetic and kinetic investigation of the role of different atomic grain boundaries in healing radiation damage in nickel," J. Mater. Sci., vol. 51, no. 2, pp. 1017–1031, 2016, doi: 10.1007/s10853-015-9432-z.

[7] K. Jin, W. Guo, C. Lu, M. W. Ullah, Y. Zhang, W. J. Weber, et al., "Effects of Fe concentration on the ion-irradiation induced defect evolution and hardening in Ni–Fe solid solution alloys," Acta Mater., vol. 121, pp. 365–373, 2016, doi: 10.1016/j.actamat.2016.09.025.

[8] P. Changizian, Z. Yao, C. Lu, F. Long, and M. R. Daymond, "Radiation effect on nano-indentation properties and deformation mechanisms of a Ni-based superalloy X-750," J. Nucl. Mater., vol. 515, pp. 1–13, 2019, doi: 10.1016/j.jnucmat.2018.11.040.

[9] M. Moradi, G. H. Farrahi, and M. Chamani, "Effect of microstructure on crack behavior in nanocrystalline nickel using molecular dynamics simulation," Theor. Appl. Fract. Mech., vol. 104, Art. no. 102390, 2019, doi: 10.1016/j.tafmec.2019.102390.

[10] L. Xia, J. Huang, Y. Chen, Y. Liu, K. Jin, X. Wang, et al., "Microstructure evolution and hardening behavior in FCC Ni under ion irradiation: Influence of dose rate," Scr. Mater., vol. 259, Art. no. 116546, 2025, doi: 10.1016/j.scriptamat.2025.116546.

[11] X. Xiao, H. Chu, and H. Duan, "Effect of grain boundary on the mechanical behaviors of irradiated metals: A review," Sci. China Phys. Mech. Astron., vol. 59, no. 6, Art. no. 664601, 2016, doi: 10.1007/s11433-015-0486-5.

[12] M. H. Oglah, "The roadmap experiment of CdO films to heterojunction of photodetectors and solar cells," Int. J. Mech. Therm. Eng., vol. 6, no. 1, pp. 21–29, 2025, doi: 10.22271/27078043.2025.v6.i1a.74.

[13] S. Julie, K. Mariappan, C. David, N. P. Wasekar, and V. Shankar, "A study on the competition and synergy between irradiation and temperature on the texture and recrystallization of nanocrystalline nickel," Appl. Surf. Sci., vol. 638, Art. no. 158085, 2023, doi: 10.1016/j.apsusc.2023.158085.

[14] O. El-Atwani, E. Martinez, E. Esquivel, M. Efe, C. Taylor, Y. Q. Wang, et al., "Does sink efficiency unequivocally characterize how grain boundaries impact radiation damage?," Phys. Rev. Mater., vol. 2, no. 11, Art. no. 113604, 2018, doi: 10.1103/PhysRevMaterials.2.113604.

[15] B. Zhang, Z. Zhang, K. Xun, M. Asta, J. Ding, and E. Ma, "Minimizing the diffusivity difference between vacancies and interstitials in multi-principal element alloys," Proc. Natl. Acad. Sci., vol. 121, no. 5, 2024, doi: 10.1073/pnas.2314248121.

[16] C. Y. Hung, G. Vetterick, E. Hopkins, J. K. Baldwin, P. Baldo, M. A. Kirk, et al., "Insight into defect cluster annihilation at grain boundaries in an irradiated nanocrystalline iron," J. Nucl. Mater., vol. 566, Art. no. 153761, 2022, doi: 10.1016/j.jnucmat.2022.153761.

[17] N. Hashimoto, M. Ando, Y. Watanabe, and H. Tanigawa, "Sink strength of grain boundaries for point defects in irradiated ferritic/martensitic steel," Mater. Charact., vol. 217, Art. no. 114448, 2024, doi: 10.1016/j.matchar.2024.114448.

[18] C. Sun, M. Song, K. Y. Yu, Y. Chen, M. Kirk, M. Li, et al., "In situ evidence of defect cluster absorption by grain boundaries in Kr ion irradiated nanocrystalline Ni," Metall. Mater. Trans. A, vol. 44, no. 4, pp. 1966–1974, 2013, doi: 10.1007/s11661-013-1635-9.

[19] C. M. Barr, N. Li, B. L. Boyce, and K. Hattar, "Examining the influence of grain size on radiation tolerance in the nanocrystalline regime," Appl. Phys. Lett., vol. 112, no. 18, 2018, doi: 10.1063/1.5016822.

[20] P. Kalita, R. Parveen, S. Ghosh, V. Grover, Y. K. Mishra, and D. K. Avasthi, "Progress in radiation tolerant materials: Current insights from the perspective of grain size and environmental temperature," J. Alloys Compd., vol. 1012, Art. no. 178330, 2025, doi: 10.1016/j.jallcom.2024.178330.

[21] M. H. Oglah, "Analyzing the time evolution of a particle by decomposes the initial state confinement in 1D well into the lowest eigenstates energy," J. Res. Appl. Sci. Biotechnol., vol. 3, no. 2, pp. 103–107, 2024, doi: 10.55544/jrasb.3.2.17.

[22] P. Simonnin, D. K. Schreiber, and K. M. Rosso, "Predicting the temperature dependence of self-diffusion behavior in Ni-Cr alloys via molecular dynamics," Mater. Today Commun., vol. 26, Art. no. 101982, 2021, doi: 10.1016/j.mtcomm.2020.101982.

[23] B. Muntifering, S. J. Blair, C. Gong, A. Dunn, R. Dingreville, J. Qu, and K. Hattar, "Cavity evolution at grain boundaries as a function of radiation damage and thermal conditions in nanocrystalline nickel," Mater. Res. Lett., vol. 4, no. 2, pp. 96–103, 2016, doi: 10.1080/21663831.2015.1121165.

[24] G. A. Vetterick, J. Gruber, P. K. Suri, J. K. Baldwin, M. A. Kirk, P. Baldo, et al., "Achieving radiation tolerance through non-equilibrium grain boundary structures," Sci. Rep., vol. 7, no. 1, pp. 1–9, 2017, doi: 10.1038/s41598-017-12407-2.

[25] B. Amin-Ahmadi et al., "Grain boundary strain as a determinant of localized sink efficiency," Acta Mater., 2022, doi: 10.1016/j.actamat.2022.117624.

[26] J. Han, V. Vitek, and D. J. Srolovitz, "The grain-boundary structural unit model redux," Acta Mater., vol. 133, pp. 186–199, 2017, doi: 10.1016/j.actamat.2017.05.002.

[27] J. E. Nathaniel II, P. K. Suri, E. M. Hopkins, J. Wen, P. Baldo, M. Kirk, and M. L. Taheri, "Grain boundary strain as a determinant of localized sink efficiency," Acta Mater., vol. 226, Art. no. 117624, 2022, doi: 10.1016/j.actamat.2022.117624.

[28] A. P. Sutton, "Grain-boundary structure," Int. Met. Rev., vol. 29, no. 1, pp. 377–404, 1984, doi: 10.1179/imtr.1984.29.1.3.

[29] C. Jiang, N. Swaminathan, J. Deng, D. Morgan, and I. Szlufarska, "Effect of grain boundary stresses on sink strength," Mater. Res. Lett., vol. 2, no. 2, pp. 100–106, 2014, doi: 10.1080/21663831.2013.871588.

[30] G. Sharma, P. Mukherjee, A. Chatterjee, N. Gayathri, A. Sarkar, and J. K. Chakravartty, "Study of the effect of α irradiation on the microstructure and mechanical properties of nanocrystalline Ni," Acta Mater., vol. 61, no. 9, pp. 3257–3266, 2013, doi: 10.1016/j.actamat.2013.02.014.

[31] S. Julie, M. K. Dash, N. P. Wasekar, C. David, and M. Kamruddin, "Effect of annealing and irradiation on the evolution of texture and grain boundary interface in electrodeposited nanocrystalline nickel of varying grain sizes," Surf. Coat. Technol., vol. 426, Art. no. 127770, 2021, doi: 10.1016/j.surfcoat.2021.127770.

[32] M. Samaras, P. M. Derlet, H. Van Swygenhoven, and M. Victoria, "Radiation damage near grain boundaries," Philos. Mag., vol. 83, nos. 31–34, pp. 3599–3607, 2003, doi: 10.1080/14786430310001600222.